Electronic, optical, and structural properties of oligophenylene molecular crystals under high pressure: An *ab initio* investigation

Peter Puschnig,* Kerstin Hummer, and Claudia Ambrosch-Draxl
Institute of Theoretical Physics, Karl-Franzens-Universität Graz, Universitätsplatz 5, A-8010 Graz, Austria

Georg Heimel, Martin Oehzelt, and Roland Resel
Institute of Solid State Physics, Graz University of Technology, Petersgasse 16, A-8010 Graz, Austria
(Received 9 December 2002; revised manuscript received 7 March 2003; published 23 June 2003)

The goal of this *ab initio* study is to investigate the role of intermolecular interactions in molecular semiconductors. We discuss the *pressure*-dependent electronic, optical, and structural properties of biphenyl and *para*-terphenyl molecular crystals. These materials can be viewed as prototypes for conjugated molecular crystals. We optimize all internal structural parameters, including bond lengths and the molecular orientation, as a function of pressure, where the lattice parameters are taken from experiment. We compare the computed bulk modulus to available experimental data. The electronic band structures are calculated for the optimized structures and are debated as a function of pressure. We find evidence that one has to dismiss the picture of *pure* van der Waals crystals, which has been discussed in the literature for oligo-*para*-phenylenes as well as for other fundamental types of molecular crystals, such as oligothiophenes or polyacenes. Furthermore, we observe a redshift and a broadening of the optical transitions under pressure. Analysis shows that these effects are of purely intermolecular origin while changes in the internal molecular geometry are of less importance in the high-pressure regime up to 5 GPa.

DOI: 10.1103/PhysRevB.67.235321 PACS number(s): 71.15.Ap, 71.15.Mb, 71.20.Rv

I. INTRODUCTION

Ordered films of organic conjugated polymers or oligomers are not only relevant for novel optoelectronic devices but also interesting for fundamental research.[1–6] In these systems composed of quasi-one-dimensional (quasi-1D) polymer chains or molecules, which are arranged in a 3D crystalline environment, the effects of electronic confinement and the role of correlations can be studied. The vast majority of quantum chemical as well as solid-state theoretical studies, on the other hand, do not take into account the effects of crystallinity and focus on *isolated* polymers or molecules since the main optoelectronic characteristics arise from the mobile π electrons delocalized along the polymer backbone.[7–11]

In practice, polymer films consist of a distribution of different chain lengths rather than of one defined length; there is always a certain degree of misalignment of polymer chains, and there are chemical defects present, which may obstruct a straightforward interpretation of experimental results. Shorter conjugated molecules (oligomers), on the contrary, can be synthesized with a controlled number of repeat units and they crystallize in a very defined way. Therefore, we have chosen to investigate molecular crystals of conjugated molecules; more precisely, we focus on oligo-*para*-phenylenes (nP) since these materials have been demonstrated to be suitable for a number of optoelectronic applications. While biphenyl (2P) can be seen as the simplest model system for this series of materials, *para*-terphenyl (3P) and *para*-quaterphenyl (4P) are used as UV laser dyes,[12,13] in scintillation counters,[14] and as wavelength shifters,[15] whereas the longer *para*-hexaphenyl (6P) is used as active layer in thin-film organic light-emitting-diodes (LED's) showing polarized blue emission.[2,3]

Applying external pressure in these materials is a very defined way to vary the *intermolecular* distances. Since the role played by intermolecular interactions is one of the key subjects of this paper, the study of the pressure dependence of relevant properties will illuminate the issue of 1D versus 3D character in these molecular crystals. In particular, we are interested in the electronic band structures and the optical absorption versus pressure. From the band splittings and dispersions due to intermolecular wave function overlap we can deduce transport properties, while absorption spectra versus pressure illustrate the effect of intermolecular interaction on the optical properties. As a prerequisite for these investigations we determine the structural changes including molecular arrangement as well as bond lengths and angles as a function of pressure.

The paper is organized as follows. The next section gives an outline of the theoretical method that has been used. In Sec. III we describe the structural properties of 2P and 3P including the bulk modulus. Section IV discusses the electronic band structures of 2P and 3P, particularly their changes upon pressure, while Sec. V comprises optical absorption spectra versus pressure. Finally, we discuss our results in Sec. VI.

II. THEORETICAL METHOD

All calculations presented in this work are based on density functional theory (DFT). We use the full-potential linearized augmented plane-wave (LAPW) method which is an all-electron method suitable for systems with periodic boundary conditions. It has proved to be a highly accurate scheme for *ab initio* calculations within the framework of DFT. In order to reduce the number of required basis functions, we have utilized the novel APW+lo basis set[16] of the

WIEN97 code.[17] The following parameters have been chosen for the self-consistency cycles for all 2P and 3P computations. The muffin-tin radii of C and H, respectively, have been set to 1.29 and 0.75 bohr, and an $RK_{\max}$ value of 3.0 has been used. For the C atom, this amounts to a value of 5.2 for $RK_{\max}(C)$. The summations over the Brillouin zone (BZ) have been carried out utilizing the tetrahedron method and by using 12 **k** points for the self-consistency cycles and up to 1120 **k** points for the optical spectra in the full BZ. We have treated exchange and correlation effects by the generalized gradient approximated (GGA) potential due to Perdew and Wang.[18]

The pressure-dependent electronic, optical, and structural properties of the molecular crystals are obtained by the following four steps of which the first one is purely experimental and described elsewhere[19] while steps (ii)–(iv) are accomplished by *ab initio* computations outlined above.

(i) Experimental determination of the pressure-dependent lattice constants by x-ray diffraction measurements. Due to the large system size, it is not possible to optimize the lattice parameters by DFT calculations.

(ii) Minimization of the total energy within DFT for a given set of lattice parameters by optimizing all internal structural degrees of freedom, involving (a) molecular orientation as well as (b) bond lengths and angles.

(iii) Determination of the electronic band structure for the fully relaxed crystal structures in terms of Kohn-Sham energies.

(iv) Computation of the optical properties in the independent quasiparticle approximation for the optimized geometries.

III. STRUCTURAL PROPERTIES

A. Crystal structure

At room temperature and ambient pressure, biphenyl (2P), $C_{12}H_{10}$, and *para*-terphenyl (3P), $C_{18}H_{14}$, both crystallize in a monoclinic crystal structure with the space group $P2_1/a$.[20,21] This structure represents the so-called *herringbone* arrangement which is very common for planar rodlike molecules. The *n*P molecules form layers aligned parallel to the *ab* plane. The normal vectors of the molecular planes of the two inequivalent molecules enclose the herringbone angle θ, and the molecular axis is tilted with respect to the c^* axis by an angle χ. The molecular arrangement and the definition of the two angles θ and χ is also illustrated in Fig. 1.

Recently, we have studied the *pressure-dependent* lattice parameters of *n*P (2P–6P) by means of energy-dispersive x-ray powder diffraction under hydrostatic pressure up to 6 GPa.[19] As main results we obtained that (i) no phase transition occurs in the investigated pressure regime and (ii) the lattice constant *a* is reduced roughly twice as much as *b* and *c*. Although the limited number of Bragg peaks did not allow for a Rietveld refinement of the internal degrees of freedom—for instance, the molecular orientation—the strong reduction of *a* suggested a flattening of the herring bone pattern. Thus, an increase of θ was concluded but no quantitative results could be deduced from the experimental spectra. Similarly, we argued from a qualitative packing analysis that the setting angle χ should increase with pressure.[19]

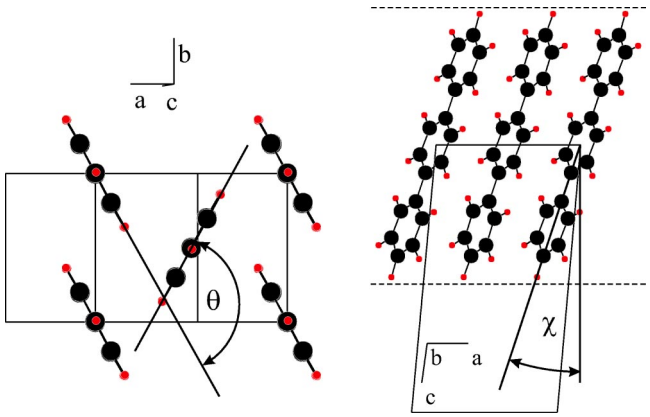

FIG. 1. The crystal structure of oligo-*para*-phenylenes is exemplified for 3P. The left panel is a projection perpendicular to the molecular axis showing the herringbone angle θ, whereas the right panel is a sideview of one such layer displaying the definition of the setting angle χ.

B. Molecular arrangement and bond lengths

The optimum molecular geometry can be obtained by minimizing the forces acting on the nuclei. However, such a scheme only works well for the *intramolecular* structure—that is, for the bond lengths and angles—while it is not practicable for a determination of the molecule's *orientation* within the unit cell. Therefore, we optimize the bond lengths and angles in a first step by utilizing the atomic *forces*. The molecules are assumed to be planar since in the pressure region we are interested in the molecules are already planarized.[22] In a second step, we minimize the total energy of the crystal with respect to the molecular orientation for *fixed* bond lengths and angles. To this end, we define two angles describing the molecular orientation. The herringbone angle θ is the angle between the two normal vectors of the molecular planes of the two inequivalent molecules, whereas the setting angle χ is given as the angle between the molecular axis and the normal to the *ab* plane (Fig. 1). Note that the molecular axis has been found to lie in the *ab* plane for 2P and 3P in the investigated pressure range; therefore, two parameters are sufficient to determine the orientation of the molecule. The optimum orientation is obtained by finding the energy minimum of the two-dimensional energy surface $E = E(\theta,\chi)$. Figure 2 shows the total energy of 2P as a function of the herringbone angle θ for a number of pressure points between 0 and 5 GPa.

We see that the optimum θ for 2P is no continuous function of pressure due to the double-well structure of $E(\theta)$, as can be seen, for instance, at 1.0 GPa. Below this pressure the minimum is in the left potential well, while at higher pressures the optimum θ lies at the right part of the double well. The optimized molecular orientations of 2P and 3P given by θ and χ together with experimental values for ambient pressure are listed in Table I. We notice that the herringbone angle θ for 3P is a monotonous function of pressure in distinction to 2P.

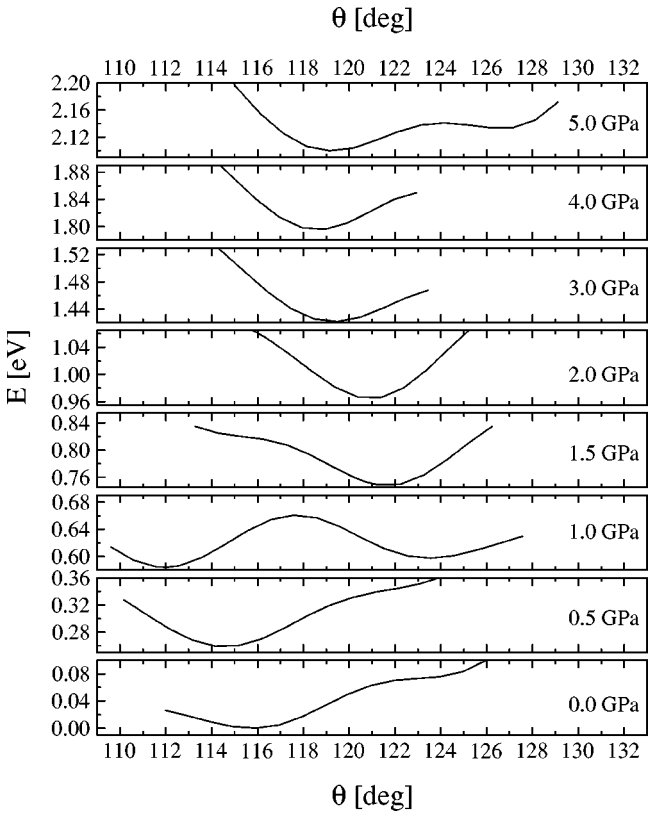

FIG. 2. Total energies E in 2P as a function of the herringbone angle θ for a number of pressure points. The origin of the energy scale has been shifted to the energy minimum of the 2P crystal structure at 0 GPa.

As a function of pressure, the herringbone angle θ shows the strongest dependence. We find more coplanar configurations at higher pressures for 2P as well as for 3P in accordance with the large change in the lattice parameter a.[19] While there is a more or less monotonous change for 3P, there is a jump in the herringbone angle θ of 2P around 1 GPa due to the double-well structure of the energy curves $E(\theta)$ given in Fig. 2. This behavior cannot be understood within the simple geometric argument of the stronger reduction of a compared to b,[19] rather it requires a more sophisticated analysis. We will come back to this point in Sec. IV where we discuss the intermolecular bonding in terms of electron density plots. According to our computations, the setting angle χ is increased by only 3.5° and 2.1° up to 5 GPa for 2P and 3P, respectively. These values have to be compared to the experimental ones of 8.7° and 6.8° up to 6 GPa for 2P and 3P, respectively, obtained from a geometric packing argument.[19] While the tendency of increasing χ as well as the larger value for 2P compared to 3P agrees with the theoretical results, the experimental values are larger than the corresponding computed ones. This discrepancy might be due to the rigid molecule approximation in Ref. 19.

TABLE I. Calculated herringbone angle θ and setting angle χ of biphenyl (2P) and *p*-terphenyl (3P) as a function of pressure. In addition, the zero-pressure values as obtained from single-crystal structure solutions (Expt.) for 2P (Ref. 20) and 3P (Ref. 21) are given.

	2P		3P	
p [GPa]	θ [deg]	χ [deg]	θ [deg]	χ [deg]
0.0	116.0	15.7	91.3	17.6
0.5	114.2	18.7		
1.0	112.1	17.2	114.0	18.7
1.5	121.3	18.2		
2.0	121.4	18.0	121.1	18.3
3.0	119.5	17.8	120.0	18.7
4.0	119.0	19.6	127.8	19.6
5.0	119.1	19.1	125.1	19.7
Expt.	112.5[a]	17.1[a]	111.6[b]	17.6[b]

[a]Reference 20.
[b]Reference 21.

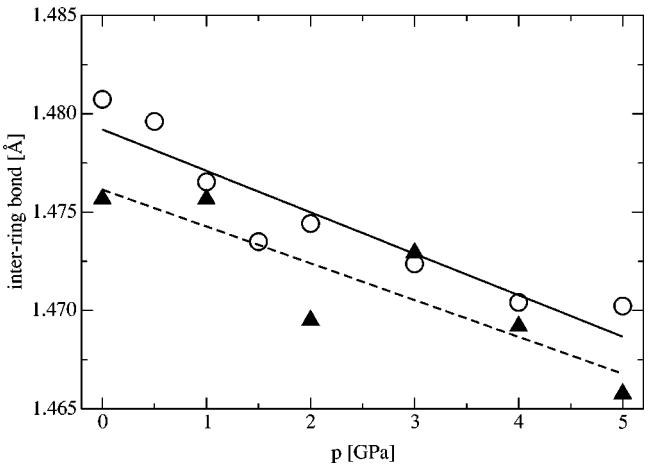

FIG. 3. The calculated interring bond length of 2P (open circles) and 3P (solid triangles) as a function of pressure. The solid (dashed) lines are linear fits to the 2P (3P) data points.

In this work, however, the internal molecular geometry (bond lengths and angles) is relaxed by making use of the atomic forces. We find, for instance, the length of one molecule defined by the end hydrogens changes by 0.05 (0.09) Å for 2P (3P) when increasing the pressure from 0 to 5 GPa. This effect can be understood in terms of the rather soft interring bonds as can be seen from a plot of the interring bond length over pressure in Fig. 3. Both for 2P and 3P, the length of the interring bond changes approximately linearly by 0.002 Å per GPa. We point out that there is no *a priori* need for a perfect linear dependence of the bond lengths versus pressure; the linear fit serves merely as a guide to the eye.

Note, however, that the change in the layer thickness given by $c \sin\beta$ is 0.52 (0.59) Å up to 5 GPa for 2P (3P), thus roughly an order of magnitude larger than the change in the length of the molecule. Consequently, the reduction of the layer thickness is mainly due to a *closer packing* of the layers since the tilting of the molecules by an angle of $\Delta\chi \approx 3°$ does not considerably decrease the layer thickness.

C. Total energies and bulk moduli

As a result of the geometry optimizations for 2P and 3P presented in the previous section, the total energies of the

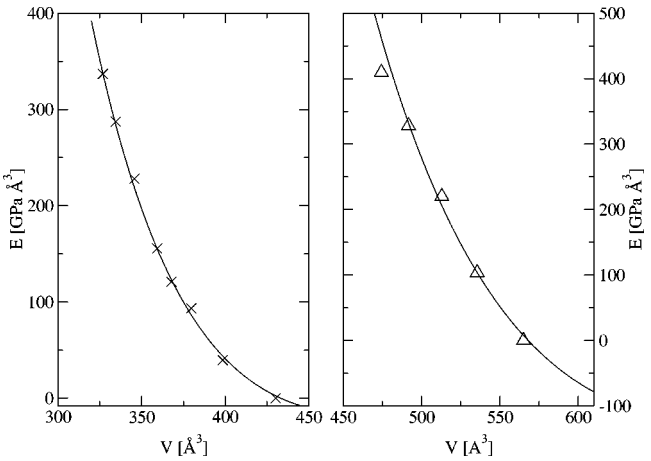

FIG. 4. The total energy E of 2P (left) and 3P (right) over the volume V. Symbols correspond to the calculated values, whereas the lines are fits according to the Birch equation of state (1). The origin of the energy scale has been shifted to the total energy at ambient pressure.

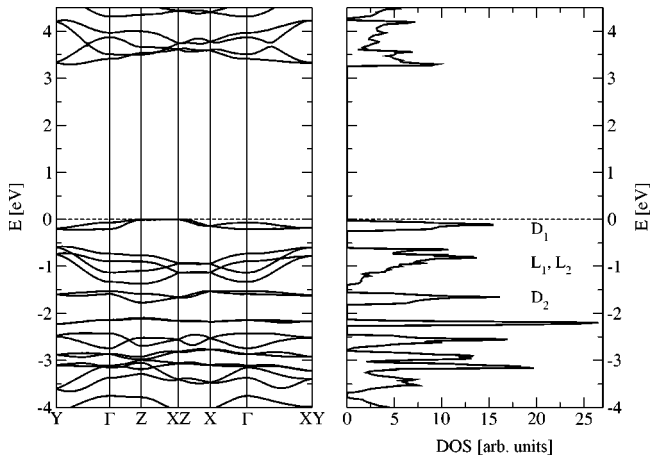

FIG. 5. The electronic band structure (left) and the density of states (right) of 2P at ambient pressure. The energetic positions of the localized (L) and delocalized (D) valence π bands are indicated. The origin of the energy scale has been set to the top of the valence band indicated by the Fermi level (dashed line).

completely relaxed structures as a function of the unit-cell volume are available. These data can be utilized to obtain the bulk modulus from a least-squares fit of the calculated total energies E as a function of volume V. We have utilized the equation of state (EOS) as proposed by Birch,[23]

$$E = E_0 + \frac{9}{8} B_0 V_0 \left[\left(\frac{V_0}{V} \right)^{2/3} - 1 \right]^2 + \frac{9}{16} B_0 V_0 (B_0' - 4) \left[\left(\frac{V_0}{V} \right)^{2/3} - 1 \right]^3, \quad (1)$$

as well as the Murnaghan EOS which has been applied to 2P and 3P previously[19,24]:

$$E = E_0 + \frac{B_0 (V - V_0)}{B_0' - 1} + \frac{B_0 V}{B_0' (B_0' - 1)} \left[\left(\frac{V_0}{V} \right)^{B_0'} - 1 \right]. \quad (2)$$

Here, B_0 and V_0, respectively, denote the zero-pressure bulk modulus and unit-cell volume, B_0' is the pressure derivative of the bulk modulus, and E_0 is the energy at zero pressure. Thus, Eqs. (1) and (2) contain four adjustable parameters which must be determined from a least-squares fit. Figure 4 displays the total energies of 2P and 3P versus the unit-cell volume as resulting from the complete relaxation of all internal structural parameters (symbols) together with a fit according to Eq. (1) (lines).

Due to the limited number of data points, a fit with all four adjustable parameters proved not to be stable. Hence, we fixed one of the parameters: namely, the pressure derivative of the bulk modulus B_0', for which we took the experimental value of $B_0' = 8.4$ ($B_0' = 6.1$) for 2P (3P) as given in Table I of Ref. 19. This procedure leads to zero-pressure volumes V_0 which are about 10% larger than the corresponding experimental ones. We have also attempted to *fix* V_0 at the experimental zero-pressure volumes, but this procedure led to the unphysical result that the bulk modulus *decreased* with pressure (negative values for B_0') if we allowed B_0' to vary or to a very bad description of the data points if we fixed B_0' at the experimental value.

The bulk moduli of 2P and 3P, respectively, resulting from the fit are $B_0 = 4.2$ GPa and $B_0 = 7.1$ GPa when using the Birch EOS and $B_0 = 1.8$ GPa and $B_0 = 5.8$ GPa when using the Murnaghan EOS. Thus, depending on the functional form of the EOS the resulting bulk modulus varies by more than a factor of 2 for 2P, while the difference is less pronounced for 3P. The large spread in the values for B_0 resulting from the Birch and Murnaghan EOS, respectively, might be explained by a systematic error in the fitting procedure. Fixing B_0' could introduce a bias in the resulting values of V_0 which affects, in turn, the calculated values for B_0. In a recent experimental study, a fit of the unit-cell volume versus pressure according to a Murnaghan EOS yielded bulk moduli of $B_0 = 4.3$ GPa and $B_0 = 7.2$ GPa for 2P and 3P, respectively. Moreover, the authors found a linear dependence of B_0 on the inverse oligomer length $1/n$ up to $n = 6$, corresponding to 6P.[19] From our calculations we find indeed that B_0 is smaller in 2P than in 3P for both EOS's in accordance with experiment.

The above discussion shows that the determination of the bulk modulus in such organic systems is not satisfactory at present and will need further considerations from the experimental as well as theoretical side. Moreover, we want to stress that these results have been obtained from DFT computations with a GGA to the exchange-correlation functional which is known not to account for van der Waals forces. We will come back to this issue in the discussion section.

IV. ELECTRONIC STRUCTURE

The electronic band structures of oligo-*para*-phenylene molecular crystals at *ambient* pressure have been discussed in some detail in previous publications.[25,26] We have depicted the band structures and densities of states (DOS) for 2P at ambient pressure and at 5 GPa in Figs. 5 and 6, respectively. Analogous plots for 3P have already been reported.[27]

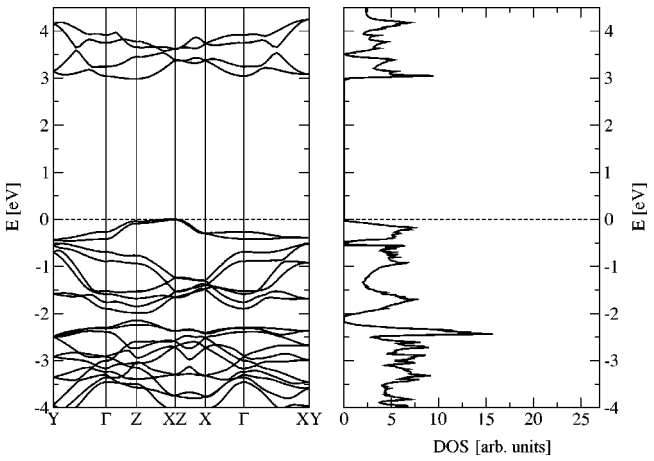

FIG. 6. The electronic band structure (left) and the density of states (right) of 2P at 5 GPa. The origin of the energy scale has been set to the top of the valence band indicated by the Fermi level (dashed line).

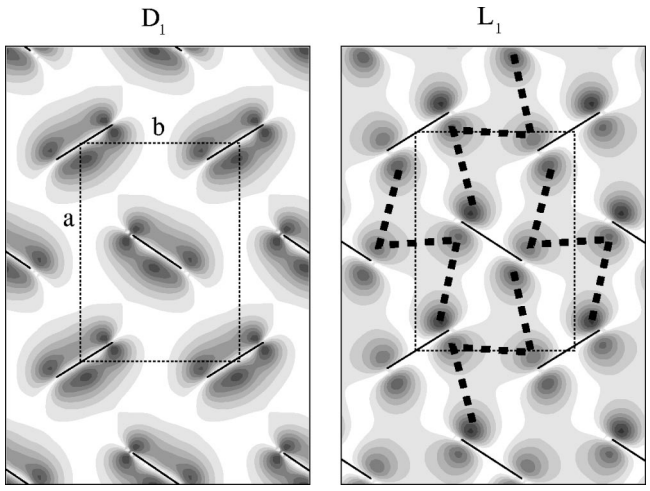

FIG. 7. The absolute value of the wave functions of the 2P delocalized (D_1) and localized (L_1) valence bands in a plane parallel to the *ab* plane. The unit-cell axes *a* and *b* are drawn as thin dashed lines while the projections of the molecules are indicated as solid lines in order to illustrate the herringbone pattern. In addition we have indicated the main directions of the intermolecular bonds for the localized state by thick dashed lines.

All band structures result from the Kohn-Sham energies; no scissors operator shift was applied.

We observe a linear reduction of the Kohn-Sham band gap for 2P (3P) from 3.25 (2.71) eV with a pressure coefficient of -50 (-40) meV/GPa. The top valence bands and bottom conduction bands can be attributed to wave functions delocalized over the whole molecule, especially over the C atoms along the long molecular axis, while the lower-lying valence bands and higher-lying conduction bands are strongly localized on the off-axis C atoms of the molecule. The energetic positions of these *delocalized* (D_1 and D_2) and *localized* (L_1 and L_2) valence bands are indicated in Fig. 5. The band dispersion is much weaker for the delocalized bands than it is for the localized ones.[35] This is due to the fact that in the herringbone structure, the localized wave functions get geometrically closer to those of the neighboring molecule than the delocalized ones do. To illustrate these circumstances we have depicted the absolute value of the wave functions at the Γ point of the BZ of a delocalized and a localized valence state in a plane perpendicular to the molecular axis in Fig. 7. In both cases the intermolecular *bonding* state of the split band doublet has been chosen.

Note that we have used the same *z* scale for both types of orbitals. While the wave function is more or less restricted to one molecule in the delocalized state, there is considerable overlap of the orbitals between neighboring molecules in the localized state. We think that the latter states are responsible for the formation of the herringbone pattern, since the herringbone arrangement maximizes the overlap of a π orbital at one molecule with the corresponding π orbitals at the neighboring two molecules. In this picture, we can understand—at least qualitatively—the zero-pressure herringbone angle θ as well as the direction of change upon increasing pressure, remembering that *a* reduces twice as much as *b*. The maximum overlap of wave functions between two molecules within the herringbone pattern can only be maintained provided that θ increases with pressure as found in Sec. III B. On the other hand, the delocalized states which determine the transport and the low-energy optical properties are little influenced by the crystalline environment. Therefore, we expect the *n*P molecular crystals to exhibit comparably small intrinsic carrier mobilities.

Similarly, we can understand that pressure affects the localized states more strongly than the delocalized ones. This can be seen from the comparison of Figs. 5 and 6 for 2P and from an analogous analysis for 3P.[27] Upon increasing the pressure from 0 to 5 GPa, the bandwidth of the top valence bands grows from 0.23 to 0.45 eV for 2P and from 0.20 to 0.32 eV for 3P, respectively; on the other hand, the localized state bandwidth increases from 0.8 (1.0) to 1.5 (1.6) eV for 2P (3P). We see that the zero-pressure bandwidth of the delocalized bands decreases upon increasing the number of rings *n*, while the opposite applies to the localized states. The former effect has also been observed in a recent quantum-chemical study of the intermolecular interactions in sexithiophene clusters.[28] Concerning the lowest *unoccupied* bands we observe an interesting effect under pressure. While at ambient pressure the lowest-lying conduction band is of delocalized character, the localized state shifts below the former at higher pressures and becomes the lowest conduction band. This is true for 2P as well as for 3P. This should result in a considerable and nonuniform increase of the electron mobility of *n*P crystals under pressure. Moreover, the band dispersion perpendicular to the long molecular axis is much stronger than it is parallel to the molecules. This is a result of the fact that the intermolecular interaction is much stronger within one layer than it is between layers.

V. OPTICAL PROPERTIES

We have calculated the imaginary part of the dielectric function (DF) in the independent particle approximation.[29] Possible limitations of this approximation will be discussed in the last paragraph of the discussion section. The optimized

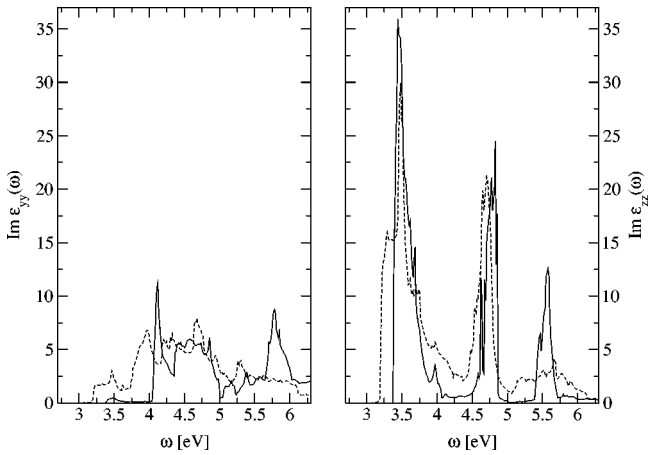

FIG. 8. The dielectric function of 2P at 0 (solid lines) and 5 (dashed lines) GPa. The left and right panels, respectively, display the *yy* and *zz* components of the imaginary part of $\epsilon(\omega)$, where the *yy* (*zz*) axis is perpendicular (parallel) to the molecular axis.

crystal structures of 2P and 3P as a function of pressure, as presented in Sec. III B, serve as input for the computation of the Kohn-Sham energies and transition matrix elements. The results for 2P at 0 and 5 GPa are displayed in Fig. 8, while the 3P spectra have been published previously.[27]

The left panel shows the *yy* components of the imaginary part of the DF for 0 and 5 GPa, whereas the right panel displays their *zz* components. Because the molecular axis lies in the *ac* plane and is approximately parallel to the *c* axis, the *yy* (*zz*) component describes absorption processes for light polarized perpendicular (parallel) to the molecular axis. The strong *zz*-polarized, lowest-energy absorption feature around 3.5 eV is formed by transitions from delocalized valence to delocalized conduction bands. The transitions involving localized bands and delocalized states, on the other hand, are *yy* polarized. The general pressure effect on the dielectric function is (i) a broadening due to increased bandwidths and (ii) a redshift due to (symmetric) band broadening of both valence and conduction bands. Both effects are clearly observed in Fig. 8.

We also checked whether the observed red shifts in the absorption are due to changes of the molecular geometry (*intramolecular*) or due to the enhanced *intermolecular* interactions. To this end, we have performed single-molecule calculations for the 2P and 3P molecules extracted from the fully optimized crystal structures.[36] By this we obtain optical transition energies versus pressure for isolated molecules having bond lengths and angles as in the corresponding crystalline environment but *without* including intermolecular effects. We find that the pressure-induced changes in these transition energies are negligibly small for both 2P and 3P. The change in the transition energies for the *isolated* molecules is below 1% in the pressure range from 0 to 5 GPa, while intermolecular effects result in redshifts between 3.5% and 10% depending on the polarization. From this we conclude that the pressure effect seen in Fig. 8 is of purely intermolecular origin, while the pressure-induced changes in the internal molecular geometry do not significantly alter the optical response of the system. The redshift of the absorption edge is much more pronounced for the *yy* component (0.7 eV) as compared to the *zz* component (0.2 eV) since the localized bands involved in the *yy* polarized transition are far more sensitive to the pressure than the delocalized ones. Similar findings are made for 3P. Here, the *yy* and *zz* components, respectively, are shifted by 0.5 eV and 0.1 eV towards the red upon increasing the pressure from 0 to 5 GPa.[27] Thus, the pressure effect on the optical absorption edges, for both *yy* and *zz* polarization, reduces upon increasing the oligomer length *n*.

VI. DISCUSSION AND OUTLOOK

The internal molecular geometry as well as the orientation of 2P and 3P in their crystalline environment is computed by minimizing the total energy within the framework of DFT. The dominating effects under pressure are (i) an increase of the herringbone angle, resulting in a more planar arrangement of the molecules, and (ii) a reduction of the interring bond length, thereby enhancing the π conjugation of the molecules. Unfortunately, we cannot directly compare these theoretical predictions to experiment, since the limited number of diffraction peaks did not allow for a Rietveld refinement of the internal structural parameters.[19] We have, however, confidence in our results since similar calculations for anthracene molecular crystals under pressure have proved to describe the molecular orientation correctly.[30–32]

As a second result, we obtain the bulk moduli B_0 of 2P and 3P from a fit of the DFT total energies to the EOS proposed by Birch and Murnaghan according to Eqs. (1) and (2). This procedure leads to values for the bulk moduli that are in reasonable agreement with recent experimental findings although the error in the theoretical result is estimated to be quite large as can be seen from the discrepancy in the Birch versus Murnaghan results.

Molecular crystals such as 2P or 3P are thought to be typical van der Waals crystals; that is, the bonding between the molecules is accomplished by rather weak dispersion forces. On the other hand, the (semi)local GGA is known to lack contributions originating from nonlocal, dynamical charge fluctuations. Therefore, we believe that we have to dismiss the picture of *pure* van der Waals crystals, which has been discussed in the literature for oligo-*para*-phenylenes as well as for other molecular crystals, such as oligothiophenes or polyacenes. This is evidenced by the noticeable overlap of wave functions between neighboring molecules within layers leading to considerable intermolecular band dispersions as discussed in Sec. IV. Moreover, it seems that the herringbone pattern of the molecules can be explained in terms of the molecular arrangement that is maximizing this intermolecular overlap.

Optical properties are discussed within the independent particle approximation. We find a redshift and a broadening of the transitions under pressure. Analysis shows that these effects are of purely intermolecular origin and changes in the molecular geometry are of less importance in the high-pressure regime up to 5 GPa. This is somewhat opposite to what has been found for the low-pressure region up to about 0.5 GPa, where the planarization of the *n*P molecules is the

most dominating effect seen in the optical absorption.[22] We will attempt an outlook on expected modifications of the optical properties upon including electron-hole interactions. The most prominent effect of electron-hole correlations is the formation of bound electron-hole states below the one-particle band gap (bound excitons). Recently, it has been found that the crystalline environment drastically reduces the exciton binding energies as compared to the isolated molecule or polymer.[33] This is partly due to the enhanced screening in the 3D material since in a simple picture the exciton binding energy E_B is inversely proportional to the square of static dielectric constant. Moreover, E_B is proportional to the effective mass of the electron-hole pair.[34] According to this effective mass approximation, we expect the exciton binding energies of 2P and 3P to decrease as a function of pressure. This is because (i) the static dielectric constants *increase* with pressure since the band gaps are reduced and (ii) the effective masses *decrease* since the bandwidths grow as a function of pressure. From these qualitative arguments we anticipate excitons in 2P and 3P to evolve from moderately bound at ambient pressure towards rather weakly bound states at high pressure. A more reliable treatment of this interesting topic by solving the Bethe-Salpeter equation will be the subject of future activities. Due to the complexity of the materials and the inevitable approximations in the calculation, these theoretical investigations should go hand in hand with an experimental determination of the optical spectra of oligo-*para*-phenylenes under high pressure.

ACKNOWLEDGMENTS

P.P. acknowledges financial support from the *Österreichische Akademie der Wissenschaften* in the form of their *Doktorandenstipendium*. The work was also partially supported by Project No. P14237 of the Austrian Science Fund.

*Electronic address: peter.puschnig@uni-graz.at; URL: http://physik.uni-graz.at/~pep/

[1] C.W. Tang and S.A. VanSlyke, Appl. Phys. Lett. **51**, 913 (1987).
[2] M. Era, T. Tsutsui, and S. Saito, Appl. Phys. Lett. **67**, 2436 (1995).
[3] S. Tasch, C. Brandstätter, F. Meghdadi, G. Leising, F. Froyer, and L. Athouel, Adv. Mater. (Weinheim, Ger.) **9**, 33 (1997).
[4] C.D. Dimitrakopoulos, A.R. Brown, and A. Pomp, J. Appl. Phys. **80**, 2501 (1996).
[5] D.J. Gundlach, Y.-Y. Lin, T.N. Jackson, and D.G. Schlom, Appl. Phys. Lett. **71**, 3853 (1997).
[6] W.A. Schoonveld, J. Wildeman, D. Fichou, P.A. Bobbert, B.J. van Wees, and T.M. Klapwijk, Nature (London) **404**, 977 (2000).
[7] E. Zojer, M. Knupfer, R. Resel, F. Meghdadi, G. Leising, and J. Fink, Phys. Rev. B **56**, 10 138 (1997).
[8] J. Cornil, D. Beljonne, C.M. Heller, I.H. Campbell, B.K. Laurich, D.L. Smith, D.D.C. Bradley, K. Müllen, and J.L. Bredas, Chem. Phys. Lett. **278**, 139 (1997).
[9] E. Zojer, J. Cornil, G. Leising, and J.L. Bredas, Phys. Rev. B **59**, 7957 (1999).
[10] J. Cornil, D. Beljonne, Z. Shuai, T.W. Hagler, I. Campbell, D.D.C. Bradley, J.L. Bredas, C.W. Spangler, and K. Müllen, Chem. Phys. Lett. **247**, 425 (1995).
[11] T. Kato, K. Yoshizawa, and K. Hirao, J. Chem. Phys. **116**, 3420 (2002).
[12] V.S. Zuev, O.A. Logunov, Y.V. Savinov, A.V. Startsev, and Y.Y. Stoilov, Appl. Phys. **17**, 321 (1978).
[13] A. Corney, J. Manners, and C.E. Webb, Opt. Commun. **31**, 354 (1979).
[14] J.L. Nogues, S. Majewski, J.K. Walker, M. Bowen, R. Wojcik, and W.V. Moreshead, J. Am. Ceram. Soc. **71**, 1159 (1988).
[15] R. Tousey and I. Limansky, Appl. Opt. **11**, 1025 (1972).
[16] E. Sjöstedt, L. Nordström, and D.J. Singh, Solid State Commun. **114**, 15 (2000).
[17] P. Blaha, K. Schwarz, and J. Luitz, *WIEN97, A Full Potential Linearized Augmented Plane Wave Package for Calculating Crystal Properties* (Karlheinz Schwarz, Technische Universität Wien, Vienna, 1999).
[18] J.P. Perdew and Y. Wang, Phys. Rev. B **45**, 13 244 (1992).
[19] G. Heimel, P. Puschnig, M. Oehzelt, K. Hummer, B. Koppelhuber-Bitschnau, F. Porsch, C. Ambrosch-Draxl, and R. Resel, J. Phys. Condens. Matter **15**, 3375 (2003).
[20] G.-P. Charbonneau and Y. Delugeard, Acta Crystallogr., Sect. B: Struct. Crystallogr. Cryst. Chem. **33**, 1586 (1977).
[21] H.M. Rietveld, E.N. Maslen, and C.J.B. Clews, Acta Crystallogr., Sect. B: Struct. Crystallogr. Cryst. Chem. **26**, 693 (1970).
[22] P. Puschnig, G. Heimel, E. Zojer, R. Resel, G. Leising, M. Kriechbaum, C. Ambrosch-Draxl, and W. Graupner, Synth. Met. **116**, 327 (2001).
[23] F. Birch, J. Geophys. Res. **83**, 1257 (1978).
[24] S.N. Vaidya and G.C. Kennedy, J. Chem. Phys. **55**(3), 987 (1971).
[25] P. Puschnig, Master's thesis, Karl-Franzens-Universität, Graz/Austria, 1999.
[26] P. Puschnig and C. Ambrosch-Draxl, Phys. Rev. B **60**, 7891 (1999).
[27] P. Puschnig, G. Heimel, K. Weinmeier, R. Resel, and C. Ambrosch-Draxl, High Press. Res. **22**, 105 (2002).
[28] J. Cornil, J.-P. Calbert, D. Beljonne, R. Silbey, and J.-L. Bredas, Synth. Met. **119**, 1 (2001).
[29] R. Del Sole and R. Girlanda, Phys. Rev. B **48**, 11 789 (1993).
[30] M. Oehzelt, K. Weinmeier, G. Heimel, P. Puschnig, R. Resel, C. Ambrosch-Draxl, F. Porsch, and A. Nakayama, High Press. Res. **22**, 343 (2002).
[31] K. Hummer, P. Puschnig, and C. Ambrosch-Draxl, Phys. Rev. B **67**, 184105 (2003).
[32] M. Oehzelt, R. Resel, and A. Nakayama, Phys. Rev. B **66**, 174104 (2002).
[33] P. Puschnig and C. Ambrosch-Draxl, Phys. Rev. Lett. **89**, 056405 (2002).
[34] L.J. Sham and T.M. Rice, Phys. Rev. **144**, 708 (1966).
[35] Remember that the term delocalized refers to the wave function *within* one molecule, whereas the band dispersion is determined by the overlap *between* two neighboring molecules.
[36] Single-molecule calculations are performed using the GAUSSIAN98 code with the same DFT-local density approximation method as described in Sec. II together with the 6-31G** basis set.